Eur. Phys. J. A **23**, 445–452 (2005)
DOI 10.1140/epja/i2004-10100-3

THE EUROPEAN PHYSICAL JOURNAL A

Mechanism of the ^{12}C(^{11}B, ^{15}N)^{8}Be reaction and ^{8}Be + ^{15}N optical-model potential

A.A. Rudchik[1], A.T. Rudchik[1], A. Budzanowski[2], A. Szczurek[2,6,a], B. Czech[2], T. Czosnyka[3], T. Choiński[3], L. Głowacka[4], S. Kliczewski[2,b], E.I. Koshchy[5], S.Yu. Mezhevych[1,7], A.V. Mokhnach[1], O.A. Momotyuk[1], Val.M. Pirnak[1], R. Siudak[2], and I. Skwirczyńska[2]

[1] Institute for Nuclear Research, Prospect Nauki 47, 03680 Kiev, Ukraine
[2] H. Niewodniczański Institute of Nuclear Physics, ul. Radzikowskiego 152, PL-31-342 Cracow, Poland
[3] Heavy Ion Laboratory of Warsaw University, ul. L. Pasteura 5A, PL-02-093 Warsaw, Poland
[4] Institute of Applied Physics, MUT, ul. Kaliskiego 2, PL-00-908 Warsaw, Poland
[5] Kharkiv National University, pl. Svobody 4, 61077 Kharkiv, Ukraine
[6] University of Rzeszów PL-35-959 Rzeszów, Poland
[7] A. Soltan Institute for Nuclear Studies, ul. Hoża 69, PL-00-681 Warsaw, Poland

Received: 21 April 2004 / Revised version: 19 October 2004 /
Published online: 20 December 2004 –
Communicated by A. Molinari

Abstract. Angular distributions of the ^{12}C(^{11}B,^{15}N)^{8}Be reaction were measured at the energy $E_{\rm lab}(^{11}{\rm B}) = 49$ MeV for the transitions to the ground and 2.94 MeV (2^+) excited state of ^{8}Be and to the ground and 5.270 MeV ($5/2^+$) + 5.299 MeV ($1/2^+$), 6.324 MeV ($3/2^-$), 7.155 MeV ($5/2^+$) + 7.301 MeV ($3/2^+$), 7.567 MeV ($7/2^+$) excited states of ^{15}N. The data were analyzed by the coupled-reaction-channel method. The elastic, inelastic scattering and one- and two-step transfers were included in the coupling scheme. The data of the ^{12}C(^{11}B,^{8}Be)^{15}N reaction at $E_{\rm cm} = 9.4$–17.8 MeV known from the literature, were also included in the analysis. The mechanism of the ^{12}C(^{11}B,^{15}N)^{8}Be reaction and the optical-model potential parameters for the ^{15}N + ^{8}Be channel were deduced. The energy dependence of the optical-model parameters for the ^{15}N + ^{8}Be channel was obtained.

PACS. 24.10.Ht Optical and diffraction models – 24.10.Eq Coupled-channel and distorted-wave models – 25.45.Hi Transfer reactions – 21.10.Jx Spectroscopic factors

1 Introduction

Multi-nucleon transfer reactions are an effective tool to study the cluster structure of interacting nuclei as well as one- and multi-step reaction mechanisms.

The ^{12}C(^{11}B,^{15}N)^{8}Be and ^{12}C(^{11}B,^{8}Be)^{15}N reactions investigated in the present work, are used to study two-step transfers including sequential nucleon and two-nucleon cluster exchanges in addition to the α- and t-cluster transfers. These reactions are also used to deduce optical-model (OM) parameters for the ^{8}Be + ^{15}N channel, which is impossible by a standard method using elastic scattering, because the ^{8}Be is unbound.

The angular distributions of the ^{12}C(^{11}B,^{15}N)^{8}Be reaction were measured for the transitions to the ground and excited states of ^{8}Be and ^{15}N at the energy $E_{\rm lab}(^{11}{\rm B}) = 49$ MeV using the ^{11}B beam from the Warsaw University cyclotron U-200P. We have found in the literature only experimental data of the ^{12}C(^{11}B,^{8}Be)^{15}N reaction for a few angles at the energies $E_{\rm cm} \approx 10$–17 MeV [1]. Those data were used together with our data to study the energy dependence of the ^{8}Be + ^{15}N OM parameters.

The data of the ^{12}C(^{11}B,^{15}N)^{8}Be and ^{12}C(^{11}B,^{8}Be)^{15}N reactions were analyzed within the coupled-reaction-channels (CRC) method using energy-dependent OM parameters for the ^{12}C + ^{11}B channel obtained in our previous work [2] from the analysis of the ^{12}C + ^{11}B elastic-scattering data. The spectroscopic amplitudes used in the CRC calculations, were successfully tested in our previous works. Thus, the angular distributions of the ^{12}C(^{11}B,^{15}N)^{8}Be and ^{12}C(^{11}B,^{8}Be)^{15}N reactions can be described by fitting OM parameters for the exit channel of ^{8}Be + ^{15}N. Analysis of the ^{12}C(^{11}B,^{15}N)^{8}Be and ^{12}C(^{11}B,^{8}Be)^{15}N reactions data for the transitions to the ground and excited states of ^{8}Be and ^{15}N provides the sets of ^{8}Be + ^{15}N OM parameters in the energy interval $E_{\rm cm} \approx 13$–29 MeV.

[a] e-mail: Antoni.Szczurek@ifj.edu.pl
[b] e-mail: Stanislaw.Kliczewski@ifj.edu.pl

These OM parameters were described by the simple functions as in our previous works (see, *e.g.*, ref. [2]) and the energy dependence of the ^{8}Be + ^{15}N OM parameters was deduced.

The paper is organized as follows. In sect. 2, we present the experimental procedure used to measure the angular distributions of the ^{12}C(^{11}B,^{15}N)^{8}Be reaction at the energy $E_{\rm lab}(^{11}{\rm B}) = 49$ MeV. Results of the CRC analysis of the ^{12}C(^{11}B,^{15}N)^{8}Be and ^{12}C(^{11}B,^{8}Be)^{15}N reactions data and the energy dependence of the ^{8}Be + ^{15}N OM parameters are presented in sect. 3. Summary and conclusions close our paper.

2 Experimental procedure

Angular distributions of the ^{12}C(^{11}B, X) reactions were measured using 49 MeV ^{11}B ion beam from the Warsaw University cyclotron U-200P. The beam energy spread was about 1%.

The reaction products were detected by the spectrometer consisting of three-window ionization chamber (ΔE-detectors) and three silicon E-detectors. The spectrometer was positioned with an accuracy of about 0.3°. The angular resolution in the lab system was $\sim 0.5°$. Argon was used as a working gas in the ionization chamber. The energy resolution of the ionization chamber was tested with α-particles from a standard radioactive source and was typically of about 2%.

The self-supporting 200 μgm/cm^2 ^{12}C foil was used as a target. No significant contaminations of heavy elements, except for ^{16}O (about 10%), in the ^{12}C target were observed. The contribution from the reaction ^{16}O(^{11}B, ^{15}N)^{12}C was subtracted in the process of data analysis.

The standard CAMAC electronics and computer acquisition system SMAN [3] were used in the present experiment. The data were stored as the $\Delta E \times E$ spectra. More experimental details were described in ref. [2].
A typical $\Delta E \times E$ spectrum is shown in fig. 1. One can see the good separation of the reaction products with charges of Z = 3–8. In contrast, the mass separation is rather poor.

A typical energy spectrum of the nitrogen isotopes obtained after extraction of continuous multi-reaction background, is shown in fig. 2. For convenience of the cross-section analysis the spectrum is presented in the energy-compressed form. The figure shows that the transitions up to the $\sim$ 7.5 MeV excited states of ^{15}N are free of contamination of other nitrogen isotopes. The peak of the 2.94 MeV level of ^{8}Be is broad. The groups of the 5.27 MeV ($1/2^+$) and 5.29 MeV ($5/2^+$) levels as well as 7.155–7.567 MeV levels of ^{15}N were not resolved in the experiment.

The energy spectra were analyzed with a code PEAKFIT, assuming symmetric Gauss shape for the peaks and suitable forms for the description of the background. In the fitting procedure the positions of peaks were fixed at the corresponding kinetic energies of the transitions. The peak widths were assumed to be equal to the width of the isolated peak at 5.3 MeV, except for the width of the broad

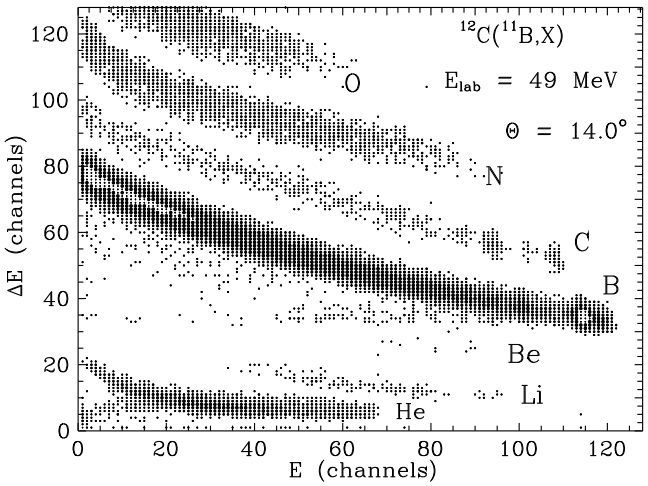

Fig. 1. A typical $E \times \Delta E$ spectrum of the ^{12}C + ^{11}B reaction products for the angle $\theta_{\rm lab} = 14°$ at the energy $E_{\rm lab}(^{11}{\rm B}) =$ 49 MeV.

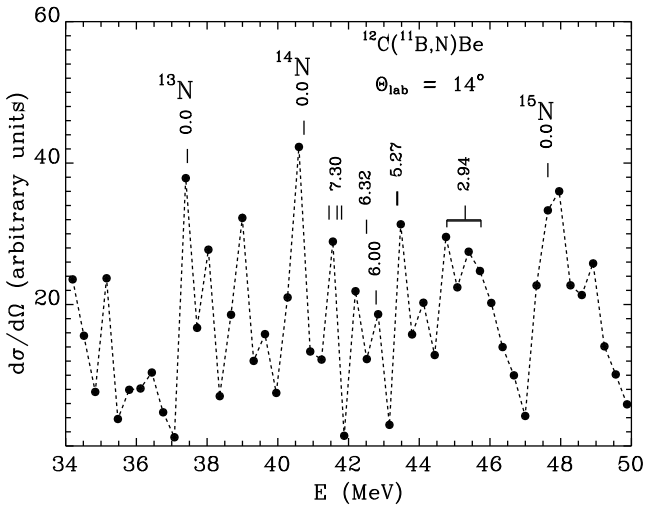

Fig. 2. A typical energy spectrum of nitrogen isotopes from the ^{12}C(^{11}B, N)Be reactions at the energy $E_{\rm lab}(^{11}{\rm B}) = 49$ MeV for the angle $\theta_{\rm lab} = 14°$.

peak corresponding to the first-excited state of ^{8}Be at the energy 2.94 MeV. Thus, only the normalization constants of Gauss forms were fitted in order to describe the energy spectra. Using such a fitting procedure, we obtained the areas under isolated and unresolved peaks with the accuracy of about 20–30%.

As a result, the angular distributions of the ^{12}C(^{11}B, ^{15}N)^{8}Be reaction at the energy $E_{\rm lab}(^{11}{\rm B}) = 49$ MeV were obtained for the transitions to the ground states of ^{8}Be and ^{15}N as well as to the 5.270 MeV ($5/2^+$) + 5.299 MeV ($1/2^+$), 6.324 MeV ($3/2^-$), 7.155 MeV ($5/2^+$) + 7.301 MeV ($3/2^+$), 7.567 MeV ($7/2^+$) excited states of ^{15}N and to the 2.94 MeV (2^+) excited state of ^{8}Be. The experimental data are shown in figs. 3-5 together with results of theoretical calculations. The errors shown in the figures include all types of uncertainties in the analysis of the spectra.

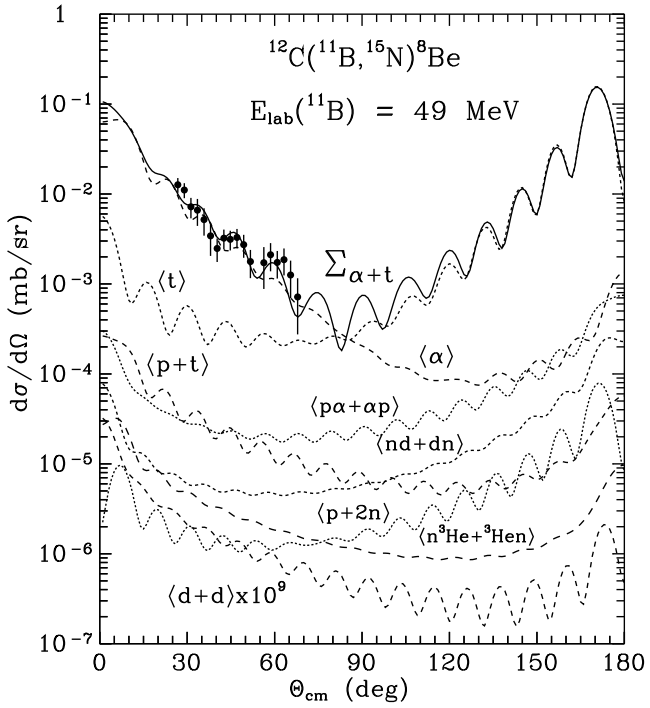

Fig. 3. Angular distribution of the ^{12}C(^{11}B,^{15}N)^{8}Be reaction for the transitions to the ground states of ^{15}N and ^{8}Be at the energy $E_{\rm lab}(^{11}{\rm B}) = 49$ MeV. The dashed curves represent the CRC cross-sections for the individual transfers or their coherent sums corresponding to the diagrams shown in fig. 7 (see text for more details). The solid curve $\Sigma_{\alpha+{\rm t}}$ shows the coherent sum of the α- and t-cluster transfers (see curves $\langle\alpha\rangle$ and $\langle{\rm t}\rangle$, respectively).

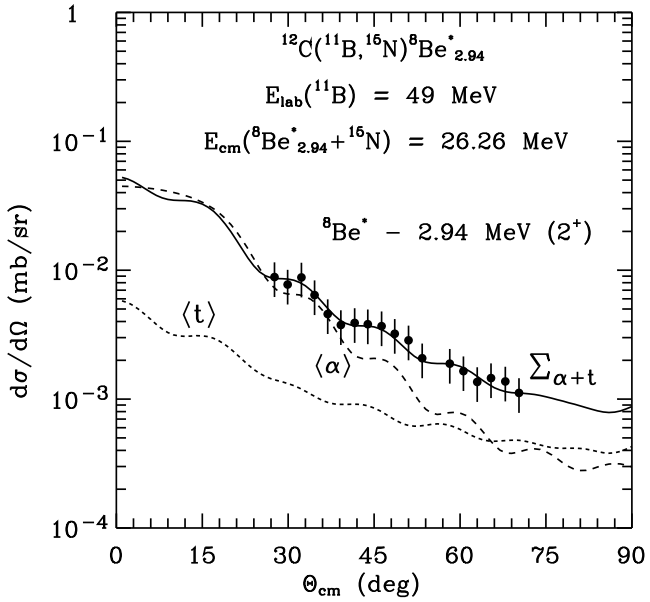

Fig. 4. Angular distribution of the ^{12}C(^{11}B,^{15}N)^{8}Be reaction at the energy $E_{\rm lab}(^{11}{\rm B}) = 49$ MeV for the transition to the 2.94 MeV (2^{+}) excited state of ^{8}Be. The dashed curves $\langle\alpha\rangle$ and $\langle{\rm t}\rangle$ present the angular distributions for the α- and t-cluster transfers, respectively. The solid curve $\Sigma_{\alpha+{\rm t}}$ shows the coherent sum of these transfers.

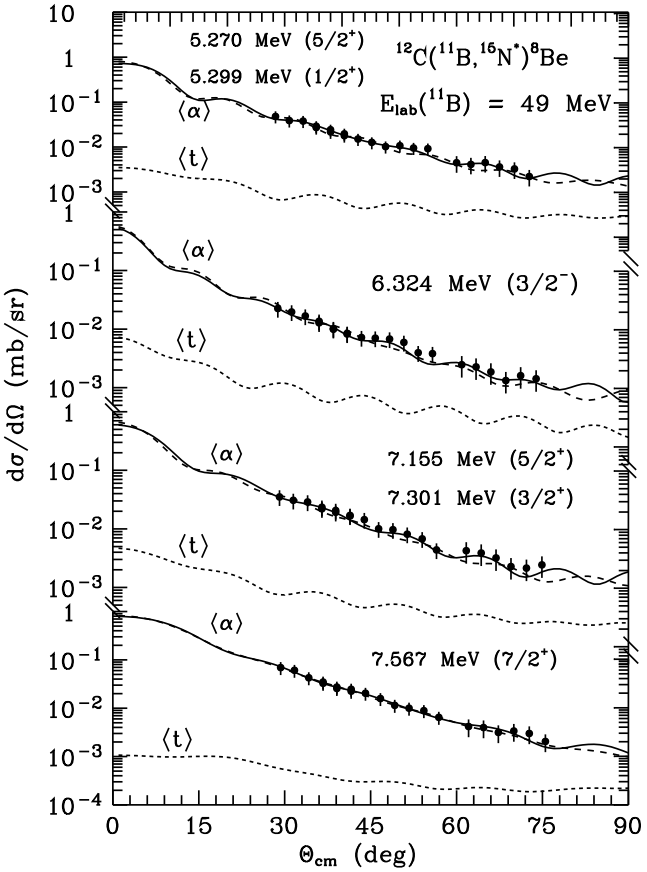

Fig. 5. Angular distributions of the ^{12}C(^{11}B,^{15}N)^{8}Be reaction at the energy $E_{\rm lab}(^{11}{\rm B}) = 49$ MeV for the transitions to the 5.27 MeV ($5/2^{+}$) + 5.299 MeV ($1/2^{+}$), 6.324 ($3/2^{-}$), 7.155 MeV ($5/2^{+}$) + 7.301 MeV ($3/2^{+}$) and 7.567 MeV ($7/2^{+}$) excited state of ^{15}N. The angular distributions for the α- and t-cluster transfers are presented by dashed curves $\langle\alpha\rangle$ and $\langle{\rm t}\rangle$, respectively. The solid curves represent the coherent sums of the α- and t-cluster transfers.

3 Analysis of the data

The angular distributions of the ^{12}C(^{11}B,^{15}N)^{8}Be reaction for the ground and excited states of ^{8}Be and ^{15}N at the energy $E_{\rm lab}(^{11}{\rm B}) = 49$ MeV ($E_{\rm cm} = 25.57$ MeV) as well as data of the ^{12}C(^{11}B,^{8}Be)^{15}N reaction at the energies $E_{\rm cm} = 10$–17 MeV [1] known from the literature, were analyzed within the coupled-reaction-channel method. The code FRESCO [4] was used for the CRC calculations.

The data of the ^{12}C(^{11}B,^{8}Be)^{15}N reaction at the c.m. energies ranging from 10 MeV up to 17 MeV in step of 1 MeV were obtained from the differential cross-sections $\sigma(\theta, E)$ given in ref. [1] at $\theta_{\rm cm} = 12.2°$, 20.0°, 36.2°, 44.2° and 52.0°. These angular distributions are shown in fig. 6.

The optical-model potentials of Woods-Saxon type

$$U(r) = Vf(r, R_V, a_V) + iW_S f(r, R_W, a_W) \qquad (1)$$

and the Coulomb potentials of a uniform charge sphere

$$V_C(r) = \begin{cases} \frac{Z_P Z_T e^2}{2R_C}\left(3 - \frac{r^2}{R_C^2}\right), & r \le R_C\ , \\ \frac{Z_P Z_T e^2}{r}, & r > R_C \end{cases} \qquad (2)$$

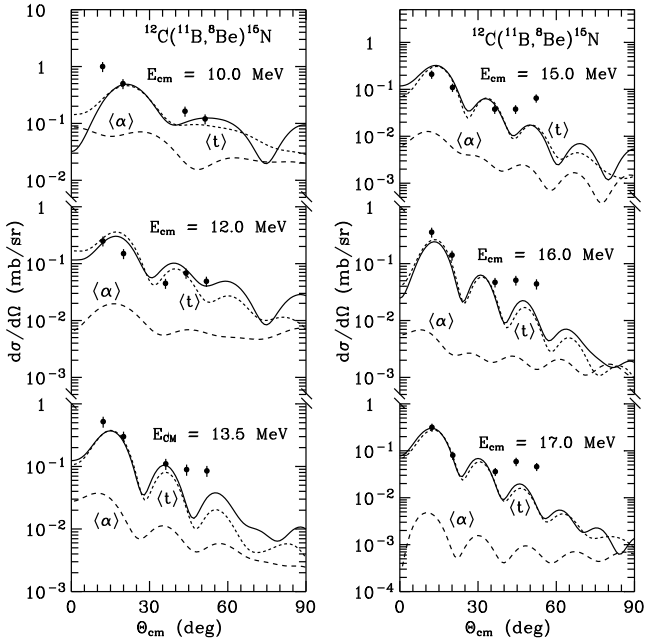

Fig. 6. Angular distributions of the ^{12}C(^{11}B,^{8}Be)^{15}N reaction at the energies $E_{\rm cm}$ = 10–17 MeV for the transitions to the ground states of ^{8}Be and ^{15}N (data from [1]). The dashed curves $\langle\alpha\rangle$ and $\langle$t$\rangle$ show the angular distributions of the α- and t-cluster transfers, respectively. The solid curves present the coherent sum of these transfers.

were used in the CRC calculations for both entrance and exit channels of the ^{12}C(^{11}B,^{15}N)^{8}Be reaction. Above

$$f(r,R_i,a_i)=\left[1+\exp\left(\frac{r-R_i}{a_i}\right)\right]^{-1},$$

$$R_i=r_i(A_P^{1/3}+A_T^{1/3}),\quad i=V,W,C,$$

Z_P, A_P and Z_T, A_T are the charge and mass numbers of projectile (or ejectile) and target (or target product), respectively.

The radius of the Coulomb potential for entrance and exit channels was fixed at the value of r_C = 1.25 fm.

The OM parameters $\{X_i\}=\{V,r_{_V},a_{_V},W_{_S},r_{_W},a_{_W}\}$ for the entrance ^{12}C + ^{11}B channel were taken from the energy-dependent parametrization obtained in ref. [2] based on elastic-scattering data. These OM parameters are listed in table 1.

The spectroscopic amplitudes S_x for a cluster x in the system $A=C+x$ needed in the CRC calculations for the ^{12}C(^{11}B,^{15}N)^{8}Be and ^{12}C(^{11}B,^{8}Be)^{15}N reactions, were obtained within the translational-invariant-shell-model (TISM) [5] with the help of the code DESNA [6,7] and A.N. Boyarkina's wave function tables [8]. These amplitudes are listed in table 2.

The $\Psi_i=|N_i[f_i](\lambda_i\mu_i)\alpha_iL_iS_iJ_iT_i\rangle$ TISM oscillatory wave functions with the $SU(3)$-symmetry $(\lambda_i\mu_i)$ (orbital part) and $SU(4)$-symmetry $[f_i]$ (spin-isospin part), describing N_i $^{(2T_i+1)(2S_i+1)}L_{iJ_i}$ states of A,C and x nuclei,

Table 1. Parameters of OM potentials (r_C = 1.25 fm).

$E_{\rm cm}$ (MeV)	V (MeV)	$r_{_V}$ (fm)	$a_{_V}$ (fm)	W_S (MeV)	$r_{_W}$ (fm)	$a_{_W}$ (fm)
		^{11}B	+	^{12}C		
10.00	114.0	0.808	0.669	4.0	1.289	0.669
12.00	147.0	0.795	0.670	4.5	1.262	0.670
13.50	175.7	0.791	0.670	5.0	1.255	0.670
15.00	202.6	0.789	0.670	5.5	1.253	0.670
16.00	217.5	0.789	0.670	5.9	1.252	0.670
17.00	229.3	0.788	0.670	6.2	1.251	0.670
25.57 [2]	241.6	0.788	0.670	9.0	1.250	0.670
		^{8}Be	+	^{15}N		
13.63	68.0	0.799	0.400	1.0	1.255	0.400
15.63	102.0	0.796	0.400	1.4	1.255	0.400
17.13	128.9	0.796	0.400	1.9	1.250	0.400
18.63	177.8	0.796	0.400	2.6	1.250	0.400
19.63	211.0	0.796	0.400	3.0	1.250	0.400
20.63	231.0	0.796	0.400	3.8	1.250	0.400
21.63	238.0	0.796	0.400	4.0	1.250	0.400
22.04	241.5	0.796	0.400	4.1	1.250	0.400
22.88	246.8	0.796	0.400	4.2	1.250	0.400
23.90	247.2	0.796	0.400	4.3	1.250	0.400
26.26	252.0	0.796	0.400	4.3	1.250	0.400
29.20	252.6	0.796	0.400	4.3	1.250	0.400

were used in the calculations of the spectroscopic amplitudes $S_x=\begin{pmatrix}A\\x\end{pmatrix}^{1/2}\langle\Psi_A|\Psi_C\Psi_x;\varphi_{Cx}\rangle$, where $i=A,C,x$; $[f_i]$ and T_i are Young tableaux and isospins, respectively, α_i are other quantum numbers, $\mathbf{J}_i=\mathbf{L}_i+\mathbf{S}_i$. The wave function $\varphi_{Cx}=|nLj\rangle$ describes the cluster x-core C relative motion. The oscillatory wave functions for the 1p-shell nuclei differ very little from the wave functions obtained with the Woods-Saxon potential. Therefore, the oscillatory spectroscopic amplitudes S_x listed in table 2 for these nuclei, are close to the more realistic ones.

Tables of ref. [8] list the energy levels $E(I,T)$ and $c_{[f]LS}$-coefficients of corresponding sets for the wave functions $\Phi_{I,T}=\Sigma c_{[f]LS}|[f]^{(2T+1)(2S+1)}L_J\rangle$ obtained within the shell model, the Hamiltonian of which includes the sum of the one-particle, pair exchange interaction and spin-orbit interaction energies. The shell model levels are in good agreement with the experimental data for most of the 1p-shell nuclei, including ^{8}Be. The spectroscopic amplitudes S_x listed in table 2 were calculated for the components of $\Phi_{I,T}$ wave functions with the maximal $c_{[f]LS}$-coefficients.

The angular distributions were calculated for the one- and two-step transfers corresponding to diagrams shown in fig. 7. First of all, the angular distributions for each individual transfer were calculated using the same OM parameters for both entrance and exit reaction channels. An individual transfer or a group of sequential transfers (*e.g.* n + d and d + n) were included in the coupling scheme together with the elastic and inelastic scattering for the transitions to the excited states of ^{11}B or ^{12}C corresponding to the diagrams presented in fig. 7. We have

Table 2. Spectroscopic amplitudes S_x for the clusters x in the $A = C + x$ systems.

A	C	x	nL_j	S_x
^{8}Be	^{7}Li	p	$1P_{3/2}$	1.234[a]
^{9}Be	^{8}Be	n	$1P_{3/2}$	0.866
^{10}B	^{8}Be	d	$1D_3$	0.811
^{11}B	^{7}Li	α	$3S_0$	−0.638
			$2D_2$	−0.422
^{11}B	^{8}Be	t	$1P_{3/2}$	0.641
^{11}B	^{8}Be$^{*}_{2.94}$	t	$2P_{1/2}$	−0.424[a]
			$2P_{3/2}$	0.424
			$1F_{5/2}$	0.148[a]
			$1F_{7/2}$	−0.363
^{11}B	^{9}Be	d	$2S_1$	−0.607[a]
			$1D_1$	−0.109[a]
			$1D_3$	0.610[a]
^{11}B	^{10}Be	n	$1P_{3/2}$	0.699
^{11}B	^{10}B	n	$1P_{3/2}$	−1.347[a]
^{12}B	^{11}B	n	$1P_{1/2}$	−0.734[a]
			$1P_{3/2}$	0.821
^{11}C	^{8}Be	^{3}He	$2P_{3/2}$	0.641
^{12}C	^{8}Be	α	$3S_0$	0.822
^{12}C	^{8}Be$^{*}_{2.94}$	α	$2D_2$	−0.919
^{12}C	^{9}Be	^{3}He	$2P_{3/2}$	1.224[a]
^{12}C	^{10}B	d	$1D_3$	1.780
^{12}C	^{11}B	p	$1P_{3/2}$	−1.706[a]
^{12}C	^{11}C	n	$1P_{3/2}$	1.706[a]
^{13}C	^{11}B	d	$2S_1$	−0.263
			$1D_1$	−0.162
			$1D_2$	−0.485[a]
^{13}C	^{12}C	n	$1P_{1/2}$	0.601
^{13}N	^{12}C	p	$1P_{1/2}$	0.601
^{14}N	^{11}B	^{3}He	$2P_{1/2}$	−0.107[a]
			$2P_{3/2}$	−0.096
			$1F_{5/2}$	−0.292[a]
^{14}N	^{12}C	d	$1D_1$	0.246
^{15}N	^{11}B	α	$2D_2$	0.435[a]
^{15}N$^{*}_{5.27}$	^{11}B	α	$3P_1$	−0.471
^{15}N$^{*}_{6.32}$	^{11}B	α	$3S_0$	−0.465
			$2D_2$	−0.308
^{15}N$^{*}_{7.15}$	^{11}B	α	$3P_1$	−0.471
^{15}N$^{*}_{7.56}$	^{11}B	α	$2F_3$	0.290[a]
^{15}N	^{12}B	^{3}He	$1P_{1/2}$	0.254[a]
			$1P_{3/2}$	−0.090
^{15}N	^{13}C	d	$2S_1$	0.248[a]
			$1D_1$	0.444[a]
^{15}N	^{12}C	t	$2P_{1/2}$	0.380
^{15}N$^{*}_{5.27}$	^{12}C	t	$1D_{5/2}$	−0.540
^{15}N$^{*}_{6.32}$	^{12}C	t	$2P_{3/2}$	0.380
^{15}N$^{*}_{7.15}$	^{12}C	t	$1D_{5/2}$	−0.540
^{15}N$^{*}_{7.56}$	^{12}C	t	$1G_{7/2}$	0.258
^{15}N	^{13}N	2n	$2S_0$	−0.608
^{15}N	^{14}N	n	$1P_{1/2}$	−1.091[a]
			$1P_{3/2}$	0.386
^{16}O	^{12}C	α	$3S_0$	0.544
^{16}O	^{15}N	p	$1P_{1/2}$	−1.461[a]

[a] $S_{\rm FRESCO} = (-1)^{J_C+j-J_A} S_x = -S_x$.

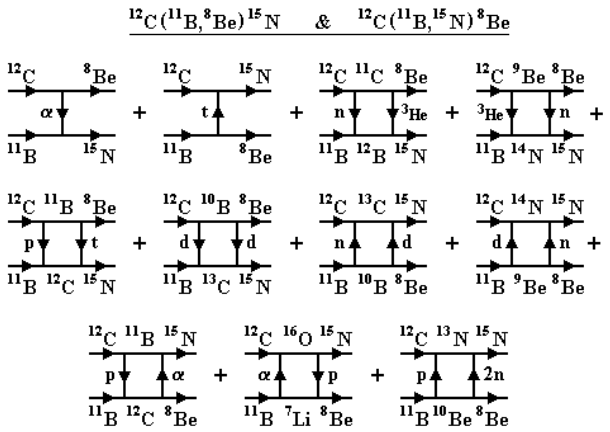

Fig. 7. Diagrams of the one- and two-step processes for the ^{12}C(^{11}B,^{15}N)^{8}Be and ^{12}C(^{11}B,^{8}Be)^{15}N reactions.

found that in the ^{12}C(^{11}B,^{15}N)^{8}Be reactions the α- and t-cluster transfers dominate at forward and backward angles, respectively, for all transitions to the ground and excited states of ^{8}Be and ^{15}N. Next, the coherent sum of α- and t-cluster transfers was fitted to the data for each transition by the variation of the OM parameters for the ^{8}Be + ^{15}N channel. As a result, the OM parameters for this channel were obtained for a few different energies. These parameters are listed in table 1. The corresponding coherent sums of the α- and t-cluster transfers are shown in figs. 3-6 by the solid curves. Below we present more details of the angular distribution analysis.

Figure 3 shows the angular distribution of the ^{12}C(^{11}B, ^{15}N)^{8}Be reaction for the transition to the ground states of ^{8}Be and ^{15}N. The curves present the CRC cross-sections for the one- and two-step transfers corresponding to the diagrams of fig. 7. One can see that the α-transfer (curve $\langle\alpha\rangle$ is dominant at forward angles where the angular distribution was measured. The t-cluster transfer is not important in this angular range. The CRC calculations predict that this transfer is dominant at backward angles (curve $\langle$t$\rangle$). The coherent sum of the α- and t-cluster transfers (solid curve $\Sigma_{\alpha+\rm t}$) describes the data satisfactorily. The sequential transfers of p + t (curve $\langle$p + t$\rangle$), p + 2n (curve $\langle$p + 2n$\rangle$), d + d (curve $\langle$d + d$\rangle$), n + ^{3}He and ^{3}He + n (curve $\langle$n^{3}He + ^{3}Hen$\rangle$ shows their coherent sum), n + d and d + n (curve $\langle$nd + dn$\rangle$), p + α and α + p (curve $\langle$pα + αp$\rangle$) contribute weakly to the ^{12}C(^{11}B,^{15}N)^{8}Be reaction.

In fig. 4 we show the angular distribution of the ^{12}C(^{11}B,^{15}N)^{8}Be reaction for the transition to the 2.94 MeV (2^+) excited state of ^{8}Be and to the ground state of ^{15}N. One can see that the α-cluster transfer (dashed curve $\langle\alpha\rangle$) dominates at the angles $\theta_{\rm cm} < 50°$ and contributions of the α- and t-cluster transfers (curves $\langle\alpha\rangle$ and $\langle$t$\rangle$, respectively) are in the region $\theta_{\rm cm} \approx 50°$–$90°$. As in the case above, the two-step transfers are negligible for this transition. The coherent sum of the α- and t-cluster transfers (solid curve $\Sigma_{\alpha+\rm t}$) describes the data satisfactorily.

The angular distributions of the ^{12}C(^{11}B,^{15}N)^{8}Be reaction at the energy $E_{\rm lab}(^{11}{\rm B}) = 49$ MeV for the transitions to the 5.270 MeV $(5/2^+)$ + 5.299 MeV $(1/2^+)$, 6.324 MeV $(3/2^-)$, 7.155 MeV $(5/2^+)$ + 7.301 MeV $(3/2^+)$ and 7.567 MeV $(7/2^+)$ excited states of ^{15}N are shown in fig. 5. The contributions of the α-cluster transfers (dashed curves $\langle\alpha\rangle$) to the data are dominant for all these transitions. In the forward hemisphere the t-cluster transfers (curves $\langle$t$\rangle$) modify the angular distributions only around $\theta_{\rm cm} = 90^\circ$. The coherent sums of the α- and t-cluster transfers (solid curves) describe all data satisfactorily. The transition to the 5.299 MeV $(1/2^+)$ excited state of ^{15}N only weakly contributes to the data of unresolved transitions to the 5.270 MeV $(5/2^+)$ + 5.299 MeV $(1/2^+)$ excited states of ^{15}N. The transition to the 7.301 MeV $(3/2^+)$ excited state of ^{15}N is also weak in comparison to the 7.155 MeV $(5/2^+)$ excited state of ^{15}N.

Experimental angular distributions of the ^{12}C(^{11}B, ^{8}Be)^{15}N reaction at the energies $E_{\rm cm} = 10$–17 MeV taken from ref. [1], are shown in fig. 6. The curves present the CRC angular distributions. One can see that in this reaction the triton transfers (dashed curves $\langle$t$\rangle$) dominate at all energies for $\theta_{\rm cm} < 90^\circ$. The α-cluster transfers (dashed curves $\langle\alpha\rangle$) only insignificantly influence the coherent sum of these transfers (see solid curves). Unfortunately, the data are very poor and a more detailed analysis is not possible. We have checked that for this reaction the two-step processes are negligible at all energies considered.

Optical-model parameters for the ^{8}Be + ^{15}N channel deduced from the CRC analysis of the ^{12}C(^{11}B,^{15}N)^{8}Be and ^{12}C(^{11}B,^{8}Be)^{15}N reactions at different energies, are listed in table 1 and presented in fig. 8 by the solid circles. These sets of the OM parameters $\{X_i\}$ for different energies were parametrized by the following functional forms (see, *e.g.*, [2] and references therein):

$$X_i(E) = \begin{cases} X_i^{\rm max} - (X_i^{\rm max} - X_i^{\rm min})\; g(E, E_{X_i}, \Delta E_{X_i}) \\ \qquad\qquad \text{for} \quad X_i = V_0, W_S, a_V, a_W, \\ X_i^{\rm min} + (X_i^{\rm max} - X_i^{\rm min})\; g(E, E_{X_i}, \Delta E_{X_i}) \\ \qquad\qquad \text{for} \quad X_i = r_V, r_W, \end{cases} \tag{3}$$

where $X_i^{\rm max}$ and $X_i^{\rm min}$ are the maximum and minimum values of the parameter X_i, respectively, $E = E_{\rm cm}$ and

$$g(E, E_{X_i}, \Delta E_{X_i}) = \left[1 + \exp\left(\frac{E - E_{X_i}}{\Delta E_{X_i}}\right)\right]^{-1}. \tag{4}$$

In the description of the energy dependence of the OM parameters the dispersion relation between the real $V(r,E)$ and imaginary $W(r,E)$ parts of the OM potential [9] was used:

$$V(r,E) = V_0(r,E) + \Delta V_W(r,E), \tag{5}$$

where

$$\Delta V_W(r,E) = \frac{\mathbf{P}}{\pi}\int_0^\infty \frac{W(r,E')}{E' - E}{\rm d}E'. \tag{6}$$

Here $\mathbf{P}$ denotes the principal value of the integral $\Delta V_W(r,E)$. At $r = 0$ formulae (5) and (6) express the relation between the depths of the real and imaginary OM potential.

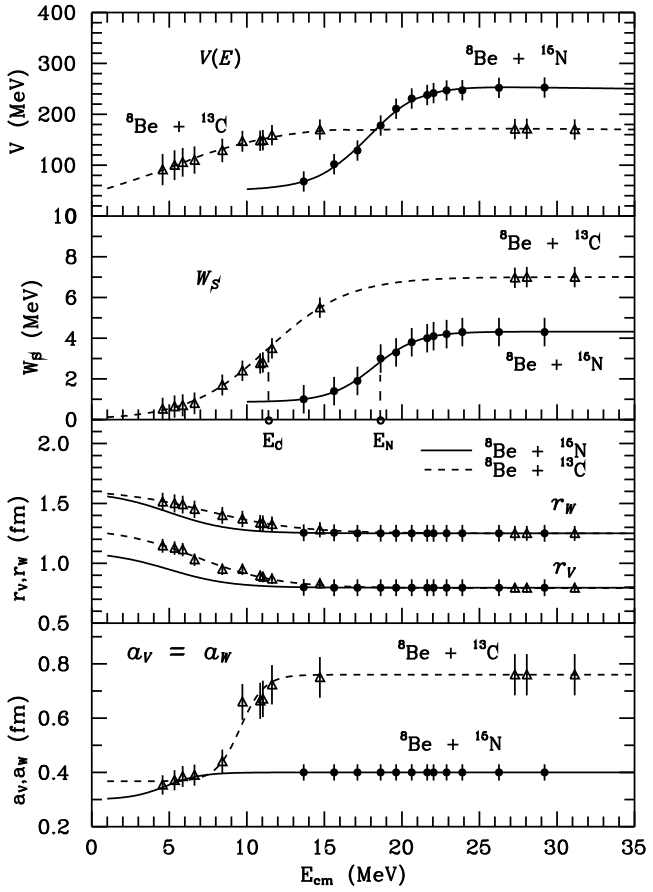

Fig. 8. Energy dependence of the OM potential parameters for the ^{8}Be + ^{13}C (open triangles and dashed curves) [10] and ^{8}Be + ^{15}N (solid circles and curves) channels.

Table 3. Energy dependence of the ^{8}Be + ^{15}N OM parameters ($E_a = 13.7$ MeV, $E_b = 21.9$ MeV)[(a)].

X_i	V_0 (MeV)	W_S (MeV)	r_V (fm)	r_W (fm)	a_V (fm)	a_W (fm)
$X_i^{\rm min}$	69.7	0.8	0.8	1.25	0.30	0.30
$X_i^{\rm max}$	270.3	4.4	1.1	1.60	0.40	0.40
E_{X_i}(MeV)	18.1	18.6	5.0	5.00	4.80	4.80
ΔE_{X_i}(MeV)	1.7	1.7	2.0	2.00	1.13	1.13

(a) E_a and E_b are parameters of the straight line approximating the exact energy dependence of W_S (see [9,10]).

The energy-dependent parameters $X_i^{\rm min}$, $X_i^{\rm max}$, E_{X_i} and ΔE_{X_i} were fitted in order to describe the energy dependences of the OM parameters X_i. As a result, the sets of the parameters $X_i^{\rm min}$, $X_i^{\rm max}$, E_{X_i} and ΔE_{X_i} were deduced for the ^{8}Be + ^{15}N channel. These parameters are listed in table 3. The corresponding energy dependences of the OM parameters are shown in fig. 8 by the solid curves.

For comparison in fig. 8 we show also the energy dependence of the OM parameters for the ^{8}Be + ^{13}C channel (open triangles and dashed curves) obtained in our

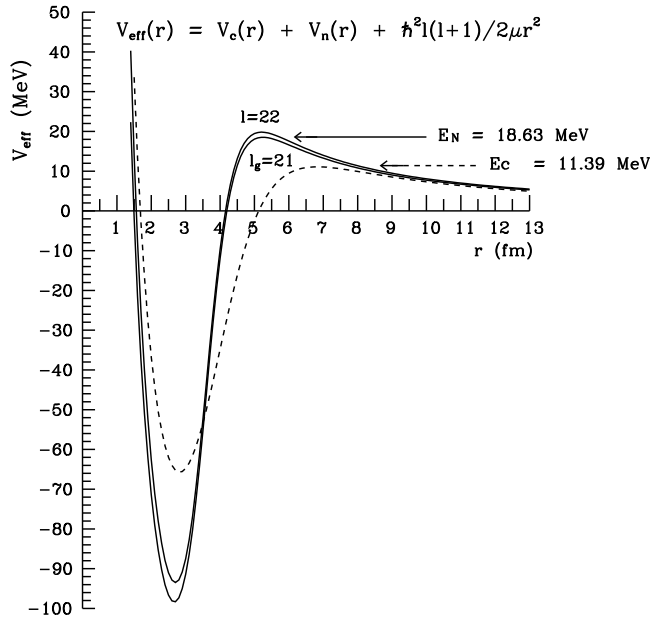

Fig. 9. Effective potential $V_{\rm eff}(r)$ for the ^{8}Be + ^{15}N (solid curves) and ^{8}Be + ^{13}C (dashed curve) channels. Parameters of the OM potential for the ^{8}Be + ^{13}C channel are taken from ref. [10].

previous work [10]. Except for $r_{_V}$ and $r_{_W}$, rather large differences between the OM parameters of the ^{8}Be + ^{13}C and ^{8}Be + ^{15}N channels can be seen.

At energies $E_{\rm cm} > 10$ MeV the parameters $a_{_V}$ and $a_{_W}$ are much smaller for the ^{8}Be + ^{15}N channel than for the ^{8}Be + ^{13}C one (see the lower panel in fig. 8). This is probably caused by closing the neutron p-shell in the ^{15}N nucleus.

The energy interval of the fast rise of W_S for the ^{8}Be + ^{15}N channel is shifted relatively to its counterpart for the ^{8}Be + ^{13}C channel (see panel for W_S in fig. 8). To characterize this shift quantitatively it is convenient to use points in the middle of the regions of the fast growths of W_S ($E_N = 18.6$ MeV for ^{8}Be + ^{15}N and $E_C = 11.39$ MeV [10] for ^{8}Be + ^{13}C). The corresponding points E_N and E_C are marked on the $E_{\rm cm}$ axis of W_S in fig. 8. The energy shift $\Delta E_{NC} = E_N - E_C = 7.21$ MeV is probably due to differences between the ^{8}Be + ^{13}C and ^{8}Be + ^{15}N potential barriers.

The fast W_S rise must correspond to an intensive opening of new inelastic channels. For nucleus-nucleus collisions inelastic processes take place mainly nearby the surfaces of interacting nuclei. Therefore, we analyze barriers of the effective potential

$$V_{\rm eff}(r) = V_C(r) + V(r) + \hbar^2 l(l+1)/2\mu r^2$$

for both interacting systems in the vicinity of grazing orbital momenta l_g. The $V_{\rm eff}(r)$ potentials were calculated using the ^{8}Be + ^{13}C OM parameters from ref. [10] at $E_{\rm cm} = 11.39$ MeV ($V_0 = 159.0$ MeV, $r_V = 0.87$ fm, $a_V = 0.723$ fm, $r_C = 0.87$ fm) and the ^{8}Be + ^{15}N OM parameters at $E_{\rm cm} = 18.63$ MeV from table 1. It was found that for both the ^{8}Be + ^{13}C and ^{8}Be + ^{15}N systems the grazing orbital momenta are $l_g = 21$. This is illustrated in fig. 9 where the effective potentials $V_{\rm eff}(r)$ are shown: dashed curve: for the ^{8}Be + ^{13}C system, solid curves: for the ^{8}Be + ^{15}N system. The grazing potential barrier for the ^{8}Be + ^{13}C system at $E_C = 11.39$ MeV is lower than for the ^{8}Be + ^{15}N system at $E_N = 18.63$ MeV. Such a difference between the grazing potential barriers for these systems is probably the reason of the energy shift of the fast growth of W_S discussed above.

The OM parameters $V(E)$ of ^{8}Be + ^{15}N and ^{8}Be + ^{13}C are also shifted in a similar way.

4 Summary and conclusions

Angular distributions of the ^{12}C(^{11}B,^{15}N)^{8}Be reaction for the transitions to the ground and 2.94 MeV (2^+) excited states of ^{8}Be and to the ground and 5.270 MeV ($5/2^+$) + 5.299 MeV ($1/2^+$), 6.324 MeV ($3/2^-$), 7.155 MeV ($5/2^+$) + 7.301 MeV ($3/2^+$), 7.567 MeV ($7/2^+$) excited states of ^{15}N were measured at the energy $E(^{11}\mathrm{B}) = 49$ MeV in the angular range $\theta_{\rm cm} < 90^\circ$ using the ^{11}B ion beam of the Warsaw cyclotron U-200P.

The present data and published earlier data of the ^{12}C(^{11}B,^{8}Be)^{15}N reaction at energies $E_{\rm cm} = 10$–17 MeV were included in the analysis within the CRC method. The one- and two-step transfers were studied. It was found that α- and t-cluster transfers dominate in the ^{12}C(^{11}B,^{15}N)^{8}Be reaction at forward and backward angles, respectively, for all transitions. For some transitions an oscillatory pattern is observed in the angular distributions around $\theta_{\rm cm} = 90^\circ$. We have found that the two-step processes are negligible in the ^{12}C(^{11}B, ^{15}N)^{8}Be and ^{12}C(^{11}B,^{8}Be)^{15}N reactions for all transitions. The coherent sums of the α- and t-cluster transfers satisfactorily describe the angular distributions of these reactions for all transitions.

Using energy-dependent OM parameters for the entrance channel of the ^{12}C(^{11}B,^{15}N)^{8}Be and ^{12}C(^{11}B,^{8}Be)^{15}N reactions and cluster spectroscopic amplitudes calculated within the translational-invariant-shell-model, the OM parameters for the ^{8}Be + ^{15}N channel were deduced from the analysis of experimental data at different energies. The energy dependence of the OM parameters for the ^{8}Be + ^{15}N channel was obtained as a result of our procedure. Differences between the energy dependence of the OM parameters for the ^{8}Be + ^{15}N and ^{8}Be + ^{13}C channels were discussed and explained by the differences of potential barriers in both channels.

This work was supported in part by the Polish State Committee for Scientific Research (Grant No. 15 PO3B 085 20). We thank Dr. hab. K. Rusek for help in the experiment as well as Prof. A. Sobiczewski and Prof. J. Jastrzębski for their interest in this work. We are indebted to the technical staff of the Heavy Ion Laboratory of Warsaw University for the good quality of the ^{11}B ion beam.

References

1. A.D. Flawley, J.F. Mateja, A. Roy, N.R. Fletcher, Phys. Rev. C **19**, 2215 (1979).
2. A.T. Rudchik, A. Budzanowski, V.K. Chernievsky, B. Czech, L. Głowacka, S. Kliczewski, A.V. Mokhnach, O.A. Momotyuk, S.E. Omelchuk, Val.M. Pirnak, K. Rusek, R. Siudak, I. Skwirczyńska, A. Szczurek, L. Zemło, Nucl. Phys. A **695**, 51 (2001).
3. M. Kowalczyk, SMAN: a Code for Nuclear Experiments, Warsaw, unpublished.
4. I.J. Thompson, Comput. Phys. Rep. **7**, 167 (1988).
5. Yu.F. Smirnov, Yu.M. Tchuvil'sky, Phys. Rev. C **15**, 84 (1977).
6. A.T. Rudchik, Yu.M. Tchuvil'sky, a code DESNA, The Kiev Institute for Nuclear Research report KIYAI-82-12 (1982).
7. A.T. Rudchik, Yu.M. Tchuvil'sky, Ukr. Fiz. Zh. **30**, 819 (1985).
8. A.N. Boyarkina, *Structure of 1p-shell Nuclei* (Moscow State University, 1973).
9. C. Mahaux, H. Ngŏ, G.R. Satchler, Nucl. Phys. A **449**, 354 (1986).
10. A.T. Rudchik, O.A. Momotyuk, A. Budzanowski, A. Szczurek, V.K. Chernievsky, A.V. Mokhnach, V.A. Ziman, E.I. Koshchy, S. Kliczewski, R. Siudak, I. Skwirczyńska, J. Turkiewicz, Nucl. Phys. A **660**, 267 (1999).